Journal of Materials Chemistry A

Generalizable, Tunable Control of Divalent Cation Solvation Structure via Mixed Anion Contact Ion Pair Formation

Journal:	*Journal of Materials Chemistry A*
Manuscript ID	TA-ART-12-2023-007613.R1
Article Type:	Paper
Date Submitted by the Author:	17-Jan-2024
Complete List of Authors:	Lavan, Sydney; Argonne National Lab, Ilic, Stefan; Argonne National Laboratory, Materials Science Division Viswanath, Shashwat; Argonne National Laboratory, Materials Science Division Jain, Akash; Argonne National Laboratory, Materials Science Division Surendran Assary, Rajeev; Argonne National Laboratory, Materials Science Division; Connell, Justin; Argonne National Laboratory, Materials Science Division

Generalizable, Tunable Control of Divalent Cation Solvation Structure via Mixed Anion Contact Ion Pair Formation

Sydney N. Lavan[1,2], Stefan Ilic[1,2], Shashwat Viswanath[1,2], Akash Jain[1,2], Rajeev S. Assary[1,2] and Justin G. Connell[1,2]*

[1] *Joint Center for Energy Storage Research, Argonne National Laboratory, Lemont, IL 60439, USA*

[2] *Materials Science Division, Argonne National Laboratory, Lemont, IL 60439, USA*

** Email: jconnell@anl.gov*

Abstract

Multivalent batteries are a promising new technology for energy storage, but they face challenges to developing suitable electrolytes that can support reversible deposition/dissolution at the metal anode and enable compatibility with high voltage oxide cathode materials. In this work, we investigate the solvation behavior of Zn^{2+}, Mg^{2+}, Ca^{2+} and Cu^{2+} in mixed anion electrolytes containing $TFSI^-$ and Cl^-. Raman and nuclear magnetic resonance spectroscopies are utilized to probe the bulk solvation structure of these electrolytes and demonstrate that mixed anion contact ion pairs (CIPs) are formed in all four systems, indicating this behavior is likely general to divalent cations. Furthermore, the relative population of mixed anion CIPs can be tuned by controlling the relative ratio of TFSI:Cl, with significant CIP populations observed even at low relative fractions of Cl^-. These findings imply that modifying the anion chemistry can easily adjust the solvation structure of bulk cations, which has important implications for the development of next-generation electrolytes. By understanding the factors that influence the formation of mixed anion CIPs, we can design systems that promote the formation of electrochemically-active solvation structures that can enable multivalent batteries with improved performance and lifetimes.

Keywords

Multivalent electrolytes; Solvation Structure; Contact ion pairs; Vibrational Spectroscopy; Zinc; Magnesium; Calcium; Copper

Introduction

The need for diverse battery materials to support the growing energy storage landscape is a significant challenge, and multivalent batteries are a promising avenue for advancement.[1–4] These batteries utilize earth-abundant, non-toxic elements like Mg^{2+}, and Zn^{2+}, which can provide comparable or higher theoretical specific capacities than existing Li-ion systems while enabling stable supply chains.[5–9] However, multivalent chemistries face challenges, such as developing suitable electrolytes that can support reversible deposition/dissolution at the metal anode and enable compatibility with high voltage oxide cathode materials. Many multivalent electrolytes developed to date rely on high chloride (Cl^-) concentrations to drive reversible redox processes at the anode, but these systems are incompatible with oxide cathodes due to parasitic reactions at high voltage. [6,10]

Recent research has shown that Cl^- reduces the overpotential for metal dissolution, which comes at the cost of a higher overpotential for metal deposition. The addition of weakly-coordinating anions, like bis(trifluoromethane sulfonyl) imide ($TFSI^-$), can enable reversible metal deposition and dissolution in mixed anion electrolytes through a cooperative effect that arises due to differences in halide-cation and TFSI-cation complex association strength.[11,12] Mixed anion electrolytes have been further shown to exhibit emergent solvation behavior, whereby $TFSI^-$ anions that do not coordinate with Zn^{2+} in isolation are induced to form contact ion pairs (CIPs) when combined with halides (e.g., Cl^-, Br^-, I^-).[11] This phenomenon was confirmed by through a combination of X-ray absorption spectroscopy (XAS), Raman spectroscopy and density functional theory (DFT) modeling. Importantly, this bulk solvation behavior was found to affect the electrochemical response in mixed anion electrolytes, where the association of halides with $TFSI^-$ was found to influence the rate at which charge/discharge may take place. These results have important implications for controlling the efficiency of metal deposition/stripping and suggest a new framework for electrolyte design, where weakly-coordinating anions can be induced to participate in the first solvation shell of the working cation in the electrolyte bulk due to the presence of a second anion. Despite this new understanding of cation speciation, it is unclear whether the emergent solvation behavior described for Zn-based systems is generalizable to other multivalent electrolytes.

In this study, we expand on our previous work by examining the extent to which solvation structure can be tuned as a function of anion and cation chemistry.[13] We primarily utilize Raman

and nuclear magnetic resonance (NMR) spectroscopies to probe the bulk solvation structures of zinc, magnesium, calcium and copper-based electrolytes containing $TFSI^-$ and varying ratios of Cl^- in diglyme (G2). Consistent with our previous work in Zn-based electrolytes[13], we identify the presence of a new vibrational mode on the low frequency side of the overall Raman peak envelope for both Mg and Ca-based electrolytes that we assign to mixed anion CIPs. This assignment is corroborated by ^{19}F NMR spectroscopy, which shows systematic shifts in the $TFSI^-$ resonance that match changes in the Raman spectra as the relative concentration of Cl^- is increased. DFT calculations indicate the additional vibrational mode for Mg-based electrolytes is consistent with a mixed anion CIP, in direct analogy with results for Zn-based electrolytes. Interestingly, Raman analysis of Cu-based electrolytes does not show the same signatures of mixed anion CIP formation, but ^{19}F NMR spectroscopy of these electrolytes again suggests that they also form mixed anion CIPs. We demonstrate that significant populations of mixed anion CIPs are formed even at relatively low Cl^- contents, and that it is possible to tune the relative population of the mixed anion CIPs for all electrolytes investigated by controlling the relative ratio of TFSI:Cl. These results point to new possibilities in controlling bulk cation solvation structures in multivalent electrolytes, where the relative fraction of electrochemically-active solvation structures can be directly tuned to modulate deposition kinetics as well as the overall electrolyte reversibility.

2. Experimental Methods

2.1 Electrolyte Preparation

$Zn(TFSI)_2$, $Mg(TFSI)_2$ $Ca(TFSI)_2$ and $Cu(TFSI)_2$ (Solvionic, 99.5%), $ZnCl_2$, $CuCl_2$ (Sigma Aldrich, anhydrous, 99.995% trace metals basis) $CaCl_2$ (Sigma Aldrich, anhydrous >97% trace metal basis) and $MgCl_2$ (Beantown Chemical, 99.99% trace metals basis) were all dried under vacuum for at least 48 hours and at temperatures ≥100°C. The solvent diglyme was dried under activated basic alumna for more than 48 hours and then distilled under vacuum over Na/K alloy. The H_2O content was less than 0.2 ppm and was determined by Karl Fischer titration. For all experiments the electrolytes were prepared in an Ar atmosphere glovebox (O_2 and H_2O < 0.5 ppm) and left to stir overnight before use.

2.2 Raman Scattering Measurements

To assess the $TFSI^-$ sensitive vibrational modes we used a Renishaw in via Reflux Raman micro-spectrometer fitted with a 20x microscope objective. The solution phase Zn^{2+} and Mg^{2+} measurements were excited at 633 nm and collected with 1800 grooves/mm diffraction grating. The solution phase Cu^{2+} measurements were excited at 532 nm due to fluorescence and collected with 1800 grooves/mm diffraction grating. We can achieve as high as 0.2 cm^{-1} spectral resolution dependent on the grating and the laser. The experimentally measured peaks for Zn^{2+} and Mg^{2+} were

determined from a combination of ~75% Lorentzian line shapes and ~25% Gaussian line shapes (Voigt) for the "free TFSI" and 50%/50% mix for the higher CIP peaks. The fluorescent backgrounds were subtracted. Each sample was prepared in a glovebox then transferred to quartz vials for Raman measurements, and the spectrometer was calibrated to a Si reference prior to each measurement. The monodentate TFSI peak for Cu^{2+} was found to fit best at 746 cm^{-1} compared to 742 cm^{-1} (Zn^{2+}, determined in our previous work [11]) and 744 cm^{-1} (Mg^{2+}, determined by Watkins and Buttry [14].

2.3 ^{19}F Nuclear Magnetic Resonance Spectroscopy

NMR spectra were recorded on a 300 MHz Bruker Avance spectrometer at ambient temperature, with D_2O capillary for locking. We kept the $TFSI^-$ concentration constant and changed the Cl^- concentration due to the low solubility of Cu salts.

2.4 Density Functional Theory Calculations

We employ first principles calculations utilizing density functional theory (DFT).[15,16] The performed DFT calculations were carried out using Gaussian software to compute optimum structures and energies. We utilized polarizable continuum model (PCM) using 7.23 as the dielectric constant for diglyme. For the structure and frequency calculations, the B3LYP/6-31+G(d) was used.[17] First, we optimized geometries of the complexes to identify the most stable configuration with the lowest ground state energy. Subsequently, we used the Freq=Raman keyword to compute the force constants and the vibrational frequencies.

3. Results and Discussion

3.1 Spectroscopic Evidence for Formation of Mixed Anion Contact Ion Pairs

We begin with Raman experimental measurements of electrolytes containing 0.1 M $ZnTFSI_2$, $MgTFSI_2$, $CaTFSI_2$ and $CuTFSI_2$ in diglyme (black curves, Figure 1). We note that the $TFSI^-$ concentration was held fixed for all electrolytes studied in Figure 1 ([$TFSI^-$] = 0.2 M), enabling us to explore fundamental interactions, ion dynamics, and solvation structures at a constant $TFSI^-$ concentration. Furthermore, we are specifically investigating contact ion pairing, which is crucial to the performance of these electrolytes and has been shown to occur even at lower concentrations.[18] As reported previously [14,19–21], these spectra can be fit using Voigt functions to determine the relative populations of different $TFSI^-$ coordination environments (see Experimental Methods for details). Specifically, these peaks have been assigned to "free" $TFSI^-$ (740 cm^{-1}), where "free" $TFSI^-$ is not strongly associated with any cation, monodentate CIPs with $TFSI^-$ (742, 743, 744 and 746 cm^{-1}) for Zn^{2+}, Ca^{2+}, Mg^{2+} and Cu^{2+}, respectively, and bidentate CIPs with $TFSI^-$ (750 cm^{-1}). Figure S2 shows an example model structure of a metal cation

coordinated to $TFSI^-$ in a mono- and bidentate configuration with an explicit G2 molecule – $M(TFSI)^{mono}(G2)$ and $M(TFSI)^{bi}(G2)$, respectively. We note that the coordination environment for Ca^{2+} (coordination number, CN = 8) is different than for Zn^{2+}, Mg^{2+} and Cu^{2+} (CN = 6).[11,21,22] The larger coordination shell for Ca^{2+} requires the use of a fourth peak at 746 cm^{-1} to fit the TFSI-only data in Figure 1c, which has been previously assigned to an additional CIP environment that is not observed for Zn^{2+} and Mg^{2+}.[21]

When Cl^- is added to the electrolyte in a 1:1 ratio with $TFSI^-$ (0.2 M total $[M^{2+}]$, Figure 1), significant additional intensity to the low frequency side of the Raman peak envelope is observed for Zn^{2+}, Mg^{2+} and Ca^{2+} electrolytes that cannot be fit by the same peaks used for the TFSI-only data. As demonstrated previously for Zn-based electrolytes, this additional, low frequency intensity can be fit with an additional peak at 738.7-738.9 cm^{-1} (Figure 1a-c). We propose that this additional vibrational mode in the Mg^{2+} and Ca^{2+} data corresponds to a mixed TFSI-Cl CIP, in direct analogy with Zn^{2+} electrolytes, which we will explore further below. We highlight that the formation of multi-anion complexes occurs even at low concentrations, which is remarkable given that such ion pairing interactions are generally not observed until much higher concentrations, such as those achieved in so-called water/solvent-in-salt or localized high concentration electrolytes. [5,23,24] Interestingly, the same trends in mixed anion CIP formation are observed at higher total cation concentrations as well (Figure S1). For TFSI-only electrolytes (Figure S1a), we observe a minor blue shift as the concentration is increased from 0.1 M to 1.0 M, which is in line with previous results for Mg^{2+} that have shown blue shifting of the Raman envelope as more CIPs are formed relative to free $TFSI^-$. Consistent with our results in more dilute electrolytes, comparison of 0.5 M TFSI-only Zn and Mg-based electrolytes with 1:1 TFSI:Cl electrolytes (Figure S1b-c) reveals that both Zn^{2+} and Mg^{2+} still exhibit a red-shifted feature, indicating these mixed anion CIP structures are present at higher concentrations as well and demonstrating that mixed anion CIP formation takes place across a broad concentration range.

We note that these results are consistent with those of Hahn et al., where Raman spectroscopy was employed to investigate the influence of solvent structure and $TFSI^-$ concentration on the formation of CIPs. [25] Specifically, the percentage of uncoordinated $TFSI^-$ appeared to be more dependent on solvent structure than concentration within the examined concentration range. This aligns with our current study, which underscores the dominant role of solvent structure in determining the extent of direct anion-cation interactions. Furthermore, the

glyme-based solvents were found to facilitate more efficient oxygen-cation coordination due to their ability to form multidentate chelate structures, as opposed to cyclic ethers with single oxygen atoms attached to bulkier ring structures. Importantly, they also noted a lack of correlation between uncoordinated $TFSI^-$ percentage differences and solvent dielectric constant, further supporting the assertion that specific solvent-cation interactions play a critical role.

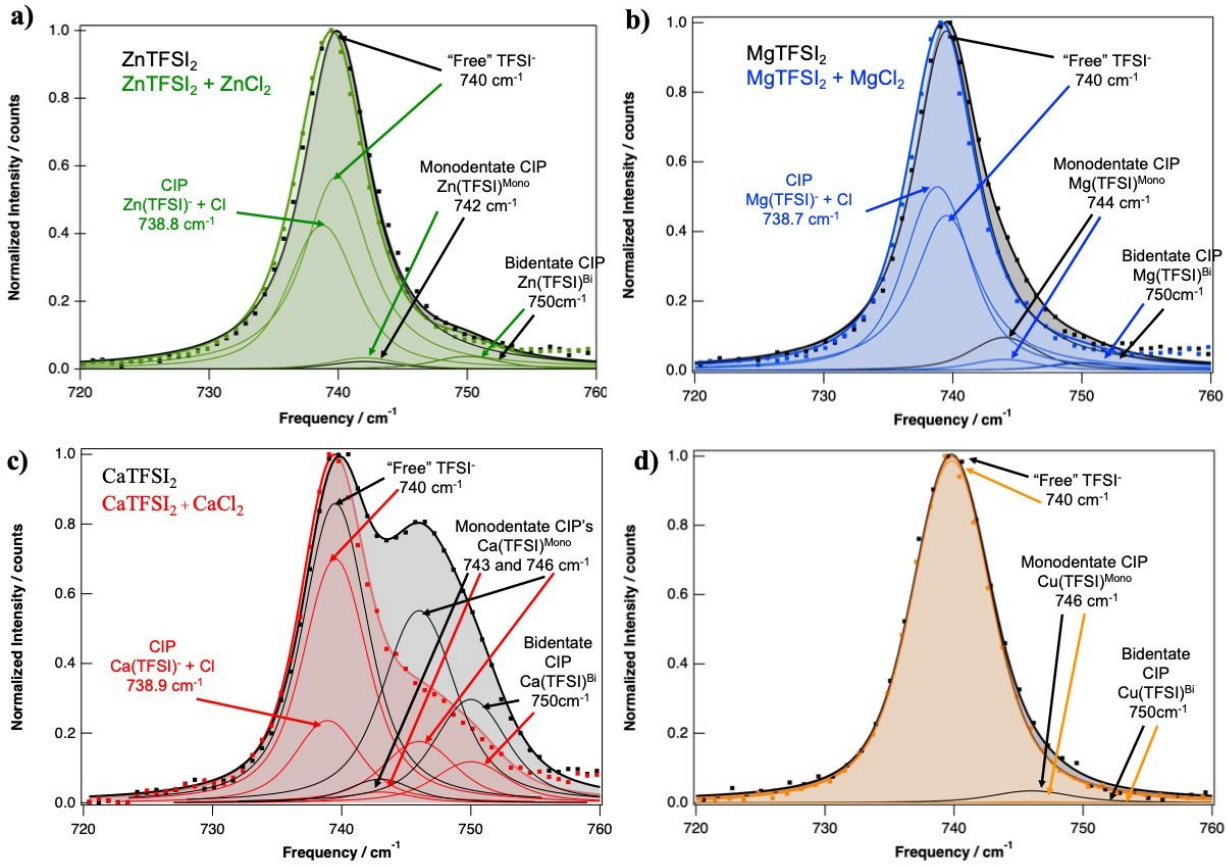

Figure 1. Raman spectroscopy (dots) and corresponding Voigt fits (lines) of the $TFSI^-$ vibrational mode comparing (a) 0.1M $ZnTFSI_2$ to mixed 0.1M $ZnTFSI_2$ + 0.1 M $ZnCl_2$ electrolytes; (b) 0.1M $MgTFSI_2$ to mixed 0.1M $MgTFSI_2$ + 0.1 M $MgCl_2$ electrolytes; (c) 0.1M $CaTFSI_2$ to mixed 0.1M $CaTFSI_2$ + 0.1 M $CaCl_2$ electrolytes (d) 0.1M $CuTFSI_2$ to mixed 0.1M $CuTFSI_2$ + 0.1 M $CuCl_2$ electrolytes.

Table 1 summarizes the relative contributions for each solvation environment for the 4 cations with $TFSI^-$ only and a 1:1 ratio of TFSI:Cl. We observe some trends when analyzing the peak contributions for each cation. For the TFSI-only electrolytes, the "free" $TFSI^-$ solvation structure dominates, as expected. In all cases monodentate CIPs generally have a higher population than bidentate. In the case of Ca^{2+}, the fraction of CIPs present is significantly higher for the TFSI-

only electrolytes than for all other cations studied. We also find for Zn^{2+}, Mg^{2+} and Ca^{2+} that the "free" $TFSI^-$ peak percentage decreases when Cl^- is present, with Mg^{2+} exhibiting a higher contribution from the mixed anion CIP peak as compared to Zn^{2+} and Ca^{2+}. The emergence of these lower frequency, mixed anion CIPs is correlated with a decrease in the intensity of the higher frequency, single anion CIP_{mono} peak in both Zn- and Mg-based electrolytes. Interestingly, Cu-based mixed anion electrolytes do not exhibit any significant changes in their Raman spectra upon the addition of Cl^- (Figure 1d). Specifically, we find that "free" $TFSI^-$ dominates for both the TFSI-only and the mixed TFSI/Cl solutions. Indeed, the only change observed is the disappearance of the monodentate CIP mode at 746 cm^{-1}, suggesting that, if present, mixed anion CIP modes are not distinguishable from the free $TFSI^-$ mode by Raman.

Table 1. Relative percent populations of the different $TFSI^-$ solvation environments determined from the fittings of experimental Raman data in Figure 1.

Solvation Structure	$ZnTFSI_2$	$ZnTFSI_2 + ZnCl_2$	$MgTFSI_2$	$MgTFSI_2 + MgCl_2$	$CuTFSI_2$	$CuTFSI_2 + CuCl_2$	$CaTFSI_2$	$CaTFSI_2 + CaCl_2$
$M(TFSI)^{mono}(Cl)$	-	40%	-	51%	-	-	-	19%
"Free" $TFSI^-$	95%	54%	89%	43%	97%	99%	48%	56%
$M(TFSI)^{mono}$	2%	3%	9%	3%	3%	0.3%	4%	2%
$M(TFSI)^{CIP}$	-	-	-	-	-	-	31%	14%
$M(TFSI)^{bi}$	3%	3%	2%	2%	0.1%	0.1%	17%	9%

3.2 Calculated Raman Spectra and Thermodynamic Favorability of Mixed Anion CIPs

Density functional theory (DFT) calculations were utilized to understand the low-frequency intensity observed in Raman spectra and other bulk solvation trends. The calculations were conducted using Gaussian's implicit solvent model with diglyme (G2) as the solvent, modeling both monodentate and bidentate CIP structures with G2 molecules present. Here we focus on Zn^{2+}, Mg^{2+} and Cu^{2+} due to the challenging nature of uniquely determining the Ca^{2+} solvation environment, particularly in mixed anion systems, due to its larger CN. Given the experimental results presented above, we suspect it would likely behave similarly, and we highlight the results of Hahn *et al.* who have already extensively considered the coordination structure of Ca in TFSI-based electrolytes. [21] Our work here focuses on monodentate CIP structures only. Results on bidentate CIPs for Zn^{2+} have been previously reported.[13]

As shown in Figure 2a, DFT calculations predict the complex breathing mode of the $TFSI^-$ anion at 765 and for $Zn(TFSI)^{mono}(G2)$. When Cl^- ions are added to these solvation structures, DFT

predicts a red shift in both modes, with the predicted red shift for the $Zn(TFSI)^{mono}(Cl)(G2)$ mode of ~4 cm^{-1} most consistent with the relative positions of the 742 and 738.8 cm^{-1} peaks observed in the experimental Raman data, as previously reported. Similar trends are observed in the case of magnesium (Figure 2b), where the $Mg(TFSI)^{mono}$ peak is predicted at 763 cm^{-1} and exhibits a ~3 cm^{-1} red shift upon the addition of Cl^-, consistent with our assignment of the low frequency mode deriving from the presence of mixed anion CIP interactions. We note that there is a smaller red-shift for $Mg(TFSI)^{mono}$ in the presence of Cl^- compared to $Zn(TFSI)^{mono}$. This ionic coordination might not be accurately captured by the DFT calculations, leading to an underestimated red-shift prediction. Furthermore, vibrational modes are generally treated as harmonic oscillators in DFT, neglecting higher-order oscillations (anharmonicities). The complex interactions between the $Mg(TFSI)^{mono}(Cl)$ CIP and its environment could induce anharmonic effects that modify the vibrational frequency, potentially contributing to the larger observed red shift in the experiment. Nevertheless, the red shifts predicted for Zn- and Mg-based mixed anion CIPs are both larger than those predicted for Cu-based CIPs (~1 cm^{-1}, Figure S4), which is consistent with the lack of any distinguishable mixed anion CIP feature in the Raman analysis of Cu-based electrolytes.

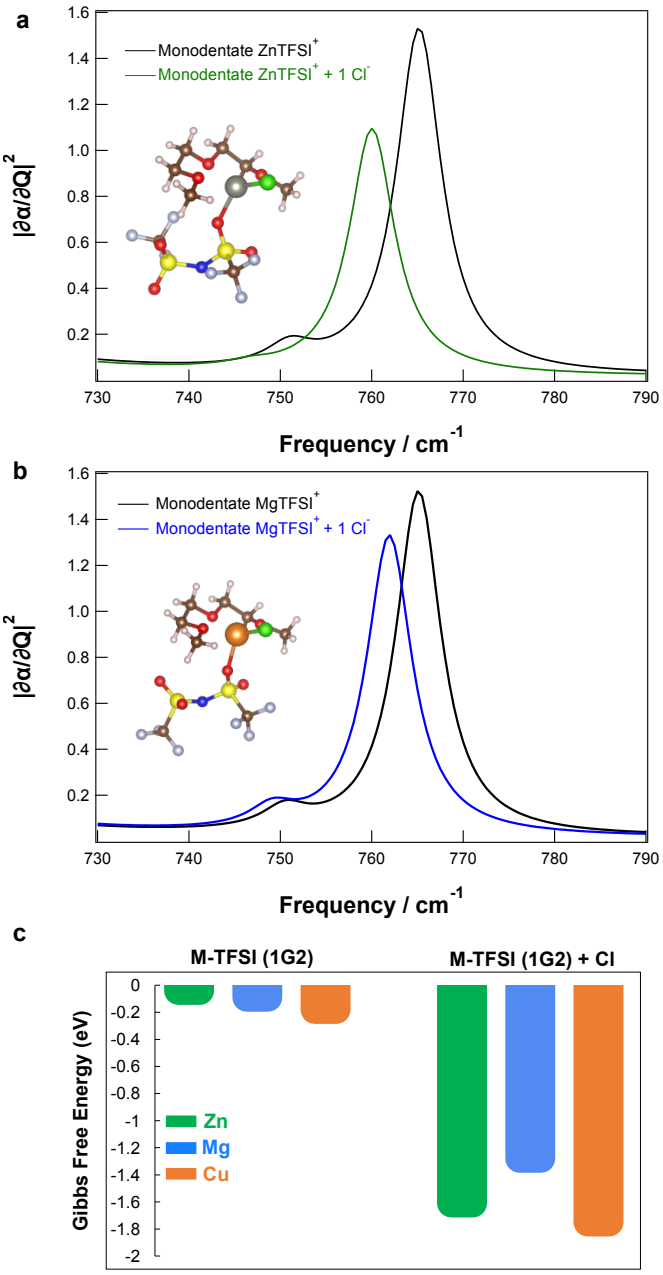

Figure 2: DFT calculated Raman spectra for (a) $Zn(TFSI)^{mono}(G2)$ and $Zn(TFSI)^{mono}(Cl)(G2)$, and (b) $Mg(TFSI)^{mono}(G2)$ and $Mg(TFSI)^{mono}(Cl)(G2)$. All structures include explicit G2. The frequencies are not scaled. (c) DFT calculated Gibbs free energy values (eV) for two modeled structures. M-TFSI in the presence of one diglyme molecule and M-TFSI + Cl in the presence of one diglyme molecule. M is the three different cations studied: zinc in green; magnesium in blue and copper in orange.

Thermodynamic calculations were performed to gain a better understanding of the relative driving forces for CIP formation and determine whether mixed anion CIPs are favorable in Zn-, Mg- and Cu-based electrolytes. The formation free energy, also known as the Gibbs free energy

of formation (ΔG), is a thermodynamic quantity that describes the energy change associated with the formation of a compound from its constituent elements, considering both enthalpy and entropy contributions. [26] We modeled two systems: the first contains each cation with $TFSI^-$ in the presence of one diglyme molecule and the second system is the same but with one Cl^- added. We note that these results do not change if a second diglyme is included in the simulation (i.e., to allow for the possibility of full octahedral coordination by the solvent). The computed ΔG values are shown in Figure 2c, and Table S1 summarizes the reactions and resulting CIP structures of all three metal ions. The free energy of contact ion pair formation is more favorable for the mixed anion system than for the pure $TFSI^-$ systems. In particular, the Gibbs free energy values for all three M-TFSI + 2 diglyme species are low (≤ -0.18 eV), consistent with the low degree of CIP formation observed experimentally in TFSI-only electrolytes for all three systems. Upon adding Cl^- to the system, the Gibbs free energy values are an order of magnitude more negative (~ -1 eV), indicating a significant thermodynamic driving force for CIP formation when Cl^- is present. We note that this is not simply an electrostatic effect due to the formation of a neutral species in the multi-anion CIP complexes. Although electrostatic interactions often play a significant role in the binding of oppositely charged ions, the system's behavior goes beyond simple charge neutralization. Additional considerations, such as the specific geometry of the coordination environment, the arrangement of anions around the metal cation in multi-anion CIPs, and electronic structure effects contribute significantly to the observed stability of the formed complexes. This implies that a comprehensive understanding of the coordination behavior in these systems requires a deeper exploration of factors beyond conventional electrostatic considerations.

Overall, these DFT results provide valuable insights into the stability and coordination behavior of Zn-, Mg- and Cu-based electrolytes with $TFSI^-$ and Cl^- in the presence of diglyme. Calculations indicate that mixed anion CIP formation is thermodynamically favorable in Mg^{2+} and Cu^{2+} electrolytes, which is in direct analogy to the Zn-based systems. Calculated Raman spectra for Mg-based CIP structures indicate a similar degree of red shifting of the $TFSI^-$ CIP modes as predicted for Zn-based CIPs. These shifts are further consistent with the position of the additional red shifted intensity observed in the experimental Raman data for Mg electrolytes, strongly suggesting that the same mixed anion CIPs identified in Zn-based mixed anion electrolytes are also formed in the Mg-based analogues. In light of the comparable Raman results observed for Ca-

based electrolytes presented above, we expect the formation of mixed anion CIP structures to be thermodynamically favorable in these electrolytes as well.

3.3 Tuning Bulk Cation Speciation

Given the lack of Raman sensitivity to mixed anion CIP formation in Cu-based electrolytes, we performed ^{19}F NMR spectroscopy to further investigate CIP formation in these mixed anion systems. Figure 3 compares the position of the $TFSI^-$ resonance for electrolytes with varying ratios of Cl^- added to a fixed concentration of $TFSI^-$. Interestingly, the position of the $TFSI^-$ resonance in TFSI-only electrolytes closely follows the solubility of the corresponding salts – i.e., $CuTFSI_2$ is the least soluble and is the most downfield shifted (-78.55 ppm); followed by $CaTFSI_2$ (-79.26 ppm), $MgTFSI_2$ (-79.35 ppm) and $ZnTFSI_2$ (-79.40 ppm). The incremental addition of corresponding chlorides to a 0.1 M solution of $M(TFSI)_2$ yields a gradual downfield shift of the ^{19}F resonance of $TFSI^-$ for Zn^{2+}, Mg^{2+} and Cu^{2+}. We have previously observed the same concentration-dependent behavior in Mg-mixed anion electrolytes [13], and we attribute these shifts to the formation of mixed anion CIPs. In particular, the $TFSI^-$ coordination environment should not otherwise be affected given that the total $TFSI^-$ concentration is held constant in all cases. Furthermore, no significant TFSI-only CIP formation is expected at this concentration (0.2 M $TFSI^-$) [5,27], nor are large populations of CIPs observed in the Raman analysis above. Combined with the clear impact of Cl^- addition on the $TFSI^-$ resonance, these results strongly indicate a multi-anion interaction that is consistent with mixed anion CIP formation.

Surprisingly, the same addition of $CaCl_2$ to $Ca(TFSI)_2$-based electrolytes yields shifts with a markedly different trend. Upon addition of 0.5 and 1 eq of $CaCl_2$, we observe an upfield shift of the $TFSI^-$ peak. The further addition of 2 equivalents of Cl^- to 0.1 M $CaTFSI_2$ results in a downfield shift of the resonance toward the TFSI-only peak position. Although the reason behind this non-linear behavior in the peak position is unclear, we speculate that it derives from the presence of the additional CIP structures formed by Ca^{2+} relative to those observed for Zn^{2+}, Mg^{2+} and Cu^{2+}, which we will explore in more detail below. Regardless of the direction of $TFSI^-$ resonance shift, however, it is evident that introduction of chlorides induces changes in the local $TFSI^-$ solvation structure. In combination with the Raman results in Figure 1, these NMR data strongly suggest that shifts in the $TFSI^-$ resonance are induced by mixed anion CIP formation.

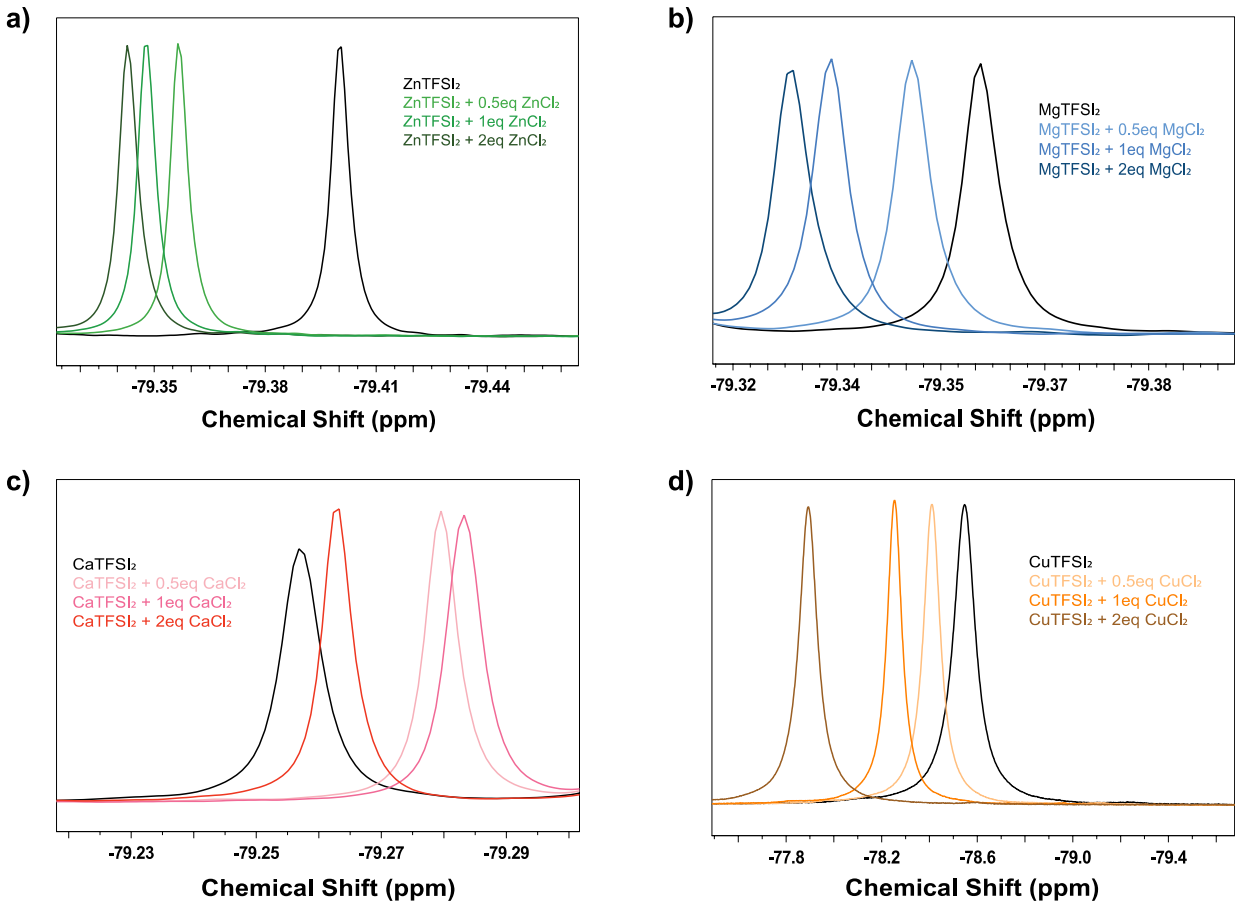

Figure 3. ^{19}NMR Spectra of the fluorine in $TFSI^-$ comparing (a) 0.1M $Zn(TFSI)_2$ with incremental addition of $ZnCl_2$; (b) 0.1M $Mg(TFSI)_2$ with incremental addition of $MgCl_2$; (c) 0.1M $Ca(TFSI)_2$ with incremental addition of $CaCl_2$; (d) 0.1M $Cu(TFSI)_2$ with incremental addition of $CuCl_2$.

Having identified the formation of mixed anion CIPs in all four electrolyte systems and to better understand the trends observed in ^{19}F NMR, we conducted further experimental Raman measurements on Zn-, Mg- and Ca-based electrolytes using the same TFSI:Cl ratios to determine the extent to which the relative fraction of mixed anion CIPs is indeed modulated by the presence of Cl^- (Figure 4). Overall, we observe that the population of mixed anion CIPs can be tuned in all three systems by the relative fraction of Cl^- present. For Zn- and Mg-based electrolytes the fraction of mixed anion CIPs reaches a maximum at a 1:1-1:2 TFSI:Cl ratio, whereas Ca-based electrolytes exhibit a peak in mixed anion CIPs at ca. 4:1-2:1 TFSI:Cl, after which the population decreases upon further Cl^- addition. Figure S5 illustrates the change in Raman spectra fitting for Mg-based electrolytes, and Tables S2, S3 and S4 provide a summary of the peak contributions for each solvation environment for all TFSI:Cl mixed ratios studied for Zn^{2+}, Mg^{2+}, and Ca^{2+}, respectively.

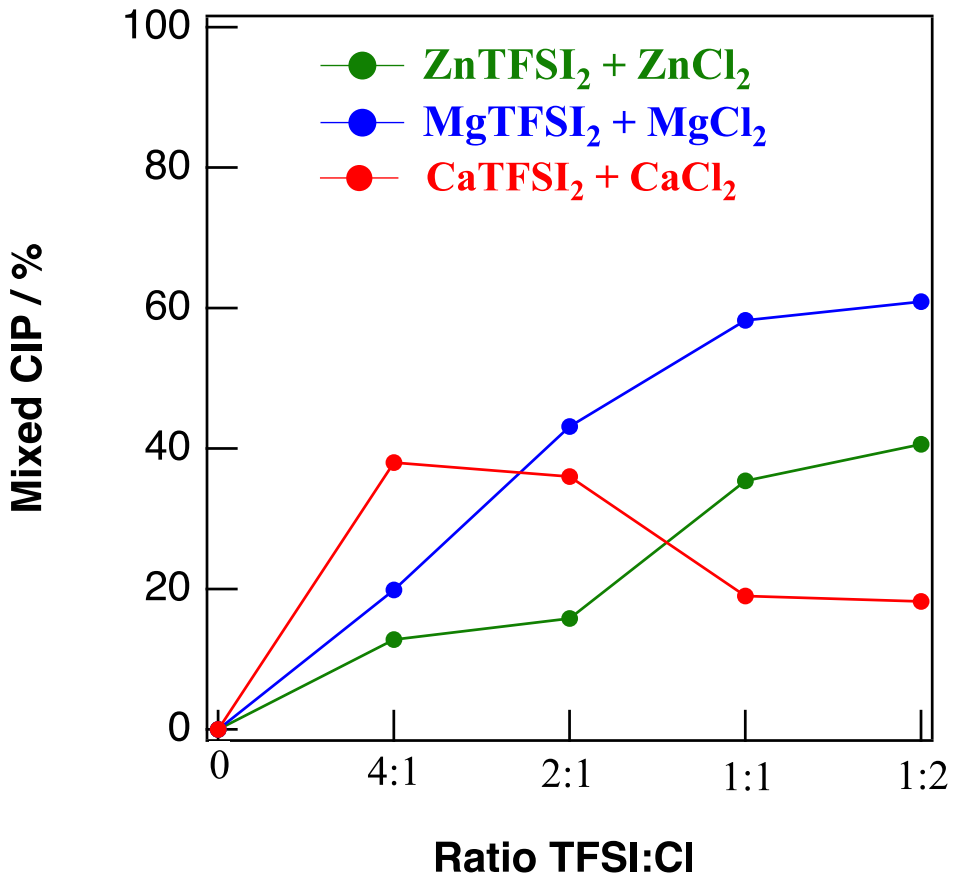

Figure 4. Experimental ratio trend of $ZnTFSI_2 + ZnCl_2$ (green), $MgTFSI_2 + MgCl_2$ (blue) and $CaTFSI_2 + CaCl_2$ (red) of the mixed CIP percentages for the different TFSI:Cl ratios investigated.

Interestingly, relatively small Cl^- additions (i.e., 4:1 TFSI:Cl) are sufficient to induce a measurable population of mixed TFSI-Cl CIPs in all three systems, with Ca-based electrolytes exhibiting the highest fraction of mixed anion CIPs at this Cl^- content. At higher Cl^- fractions, Mg-based electrolytes exhibit a larger population of mixed anion CIPs relative to Ca- and Zn-based electrolytes. We note that this higher propensity for mixed anion CIP formation in Mg-based electrolytes relative to Zn^{2+} is consistent with observations in other single anion electrolytes, including very weakly coordinating anions such as tetrakis(perfluoro-tert-butoxy) aluminate (TPFA), [28,29] suggesting that the driving force for mixed anion CIPs follows similar cation trends as single anion CIP formation. The higher charge density of Mg^{2+} may result in stronger electrostatic interactions with the Lewis basic sites on the TFSI anions, promoting the formation of stable, monodentate CIPs.[30] The increased charge density may also facilitate a more efficient utilization of coordination sites, potentially favoring the formation of monodentate complexes.

The Raman data for Ca-based electrolytes also provide a possible explanation for the shifts observed in the ^{19}F NMR data in Figure 3c. As quantified by Raman in Figure 1c and Table 1, single anion CIPs are present at substantially higher fractions in the TFSI-only Ca-based electrolytes relative to the analogous Mg-, Zn-, and Cu-based systems. The addition of Cl^- disrupts these single-anion CIP interactions by forming a new population of mixed anion CIPs (Table S4). These mixed anion CIPs likely displace some fraction of $TFSI^-$ from participating in single anion CIP structures, leading to an increase in the relative population of free $TFSI^-$ (Table S4), consistent with previous reports.[31] As the overall fraction of CIP structures is net lower, the $TFSI^-$ resonance shifts upfield as observed in Figure 3c. In contrast, for Zn^{2+}, Mg^{2+} and Cu^{2+}, the fraction of $TFSI^-$ in CIP structures increases with increasing Cl^- content at all fractions studied, leading to the consistent, downfield shifts in the $TFSI^-$ resonance observed in the NMR data in Figure 3. The exact mechanisms driving the complex evolution of Ca^{2+} coordination structures are still unclear, in particular, why the $TFSI^-$ resonance shifts back downfield upon the addition of two equivalents Cl^- without an apparent increase in the total fraction of CIPs measured by Raman. Indeed, the dynamic evolution of Ca^{2+} CIP environments are of significant interest for further investigation, but they are beyond the scope of this work. Importantly, the Raman and NMR data, along with the DFT calculations, clearly indicate that that mixed anion CIP formation is general to divalent cations, and that it is possible to tune the solvation environment by controlling the relative fractions of $TFSI^-$ and Cl^- in solution for Zn-, Mg-, Cu and Ca-based electrolytes.

Furthermore, these results can more generally explain previous observations in mixed TFSI/Cl electrolytes, as well as provide clear design rules for how to develop new multivalent electrolytes. Specifically, there are multiple examples in the literature that demonstrate the significant impact of TFSI:Cl ratio on Mg electrolyte performance[17,23,32], generally with higher Cl^- fractions yielding improved efficiency. In the context of this work, one significant driving force for these improvements in reversibility is almost certainly the increasing fraction of mixed anion CIPs in those electrolytes. In particular, disruption of the strong cation-Cl bonding of single anion CIPs by $TFSI^-$ in favor of mixed anion CIPs is likely key to maximizing the population of active complexes in the electrolyte that improve overall efficiency. We have also recently demonstrated that the formation of mixed anion CIPs in non-halide, TFSI-based dual anion systems containing trifluoromethanesulfonate (OTf^-) yields improved performance as the fraction of mixed anion CIPs increases.[13] In this mixed TFSI-OTf system, disruption of Mg-OTf single

anion CIPs (which are largely insoluble, like Cl-only CIPs) in favor of mixed anion CIPs with $TFSI^-$ is essential to improving efficiency and reversibility. The TFSI-OTf system also demonstrates that the concepts elaborated in this work are relevant well beyond halide-containing electrolytes. Overall, maximizing the population of mixed anion CIPs appears to be critical to designing dual anion electrolytes with improved performance relative to single anion analogues.

4. Conclusions

We have demonstrated the presence of mixed anion CIPs in Mg-, Ca- and Cu-based electrolytes, in direct analogy to those previously reported for Zn-based systems, and that in all systems it is possible to tune the bulk solvation structure as a function of anion chemistry. Specifically, Raman spectroscopy reveals the presence of mixed anion CIP formation in Zn-, Mg- and Ca-based electrolytes via the evolution of red-shifted intensity upon the addition of Cl^- to TFSI-containing electrolytes. Interestingly, Cu-based electrolytes do not exhibit similar features in Raman; however, ^{19}F NMR spectroscopy reveals identical shifts in the $TFSI^-$ resonance as those observed in Zn- and Mg-based electrolytes, indicating the presence of mixed anion CIPs in Cu-based electrolytes as well. DFT calculations further support the identification of the additional vibrational mode in Mg-based electrolytes as a mixed anion CIP, and thermodynamic calculations reveal that mixed anion CIP formation is thermodynamically favored in Zn-, Mg- and Cu-based systems. The relative population of mixed anion CIPs in all systems can be tuned by adjusting the TFSI:Cl ratio. In Mg^{2+}, Zn^{2+} and Ca^{2+} systems we can quantify this evolution and demonstrate that even small amounts of Cl^- are sufficient to induce a measurable population of mixed anion CIPs. These findings open possibilities for controlling the solvation structures of multivalent cations in the bulk electrolyte, enabling direct modulation of deposition kinetics and overall electrolyte reversibility. By understanding the role of anions in controlling bulk solvation behavior and demonstrating the tunability of solvation structures, this study paves the way for improved electrolyte design and the development of advanced multivalent battery systems.

Supporting Information

The SI contains Raman data for higher TFSI and mixed TFSI:Cl concentrations; tables of populations of CIP for different TFSI:Cl ratios for each cation; calculated monodentate cation

coordination structures; a summary of the implicit DFT-predicted vibrational modes; the calculated free energies and the calculated monodentate Cu-TFSI Raman spectra.

Author Contributions

Sydney N. Lavan: Conceptualization, methodology, investigation, validation, resources, writing- original draft, and visualization. Stefan Illic: Methodology, investigation, validation, resources, writing- review and editing. Shashwat Viswananth: investigation and writing- review and editing. Akash Jain: methodology, investigation, and writing – review and editing. Rajeev S. Assary: writing- review and editing, supervision. Justin G. Connell: writing- review and editing, supervision, project administration, and funding acquisition.

Acknowledgements

Experimental data collection, computational investigation and manuscript preparation was supported as part of the Joint Center for Energy Storage Research (JCESR), an Energy Innovation Hub funded by the U.S. Department of Energy, Office of Science, Basic Energy Sciences. Final data collection and manuscript preparation were supported as part of the Center for Steel Electrification by Electrosynthesis (C-STEEL), an Energy Earthshot Research Center funded by the U.S. Department of Energy, Office of Science, Basic Energy Sciences (BES) and Advanced Scientific Computing Research (ASCR). Raman spectroscopy measurements were performed at the Electrochemical Discovery Laboratory, a JCESR facility at Argonne National Laboratory. We gratefully acknowledge the computing resources provided on "Bebop", a 1024-node computing cluster operated by the Laboratory Computing Resource Center at Argonne National Laboratory. We acknowledge the use of computational resources from Center for Nanoscale Materials, an Office of Science user facility, which was supported by the U.S. Department of Energy, Office of Science, Office of Basic Energy Sciences under contract no. DE-AC02-06CH11357. We thank Dr. Haoyu Liu for assistance with NMR spectroscopy.

References

[1] L. Trahey, F.R. Brushett, N.P. Balsara, G. Ceder, L. Cheng, Y.-M. Chiang, N.T. Hahn, B.J. Ingram, S.D. Minteer, J.S. Moore, K.T. Mueller, L.F. Nazar, K.A. Persson, D.J. Siegel, K. Xu, K.R. Zavadil, V. Srinivasan, G.W. Crabtree, Energy storage emerging: A perspective

from the Joint Center for Energy Storage Research, Proc. Natl. Acad. Sci. 117 (2020) 12550–12557. https://doi.org/10.1073/pnas.1821672117.

[2] Y. Tian, G. Zeng, A. Rutt, T. Shi, H. Kim, J. Wang, J. Koettgen, Y. Sun, B. Ouyang, T. Chen, Z. Lun, Z. Rong, K. Persson, G. Ceder, Promises and Challenges of Next-Generation "Beyond Li-ion" Batteries for Electric Vehicles and Grid Decarbonization, Chem. Rev. 121 (2021) 1623–1669. https://doi.org/10.1021/acs.chemrev.0c00767.

[3] Y. Liang, H. Dong, D. Aurbach, Y. Yao, Current status and future directions of multivalent metal-ion batteries, Nat. Energy 5 (2020) 646–656. https://doi.org/10.1038/s41560-020-0655-0.

[4] J.G. Connell, B. Genorio, P.P. Lopes, D. Strmcnik, V.R. Stamenkovic, N.M. Markovic, Tuning the Reversibility of Mg Anodes via Controlled Surface Passivation by H2O/Cl– in Organic Electrolytes, Chem. Mater. 28 (2016) 8268–8277. https://doi.org/10.1021/acs.chemmater.6b03227.

[5] Y. Zhang, G. Wan, N.H.C. Lewis, J. Mars, S.E. Bone, H.-G. Steinrück, M.R. Lukatskaya, N.J. Weadock, M. Bajdich, O. Borodin, A. Tokmakoff, M.F. Toney, E.J. Maginn, Water or Anion? Uncovering the Zn^{2+} Solvation Environment in Mixed $Zn(TFSI)_2$ and LiTFSI Water-in-Salt Electrolytes, ACS Energy Lett. 6 (2021) 3458–3463. https://doi.org/10.1021/acsenergylett.1c01624.

[6] L.E. Blanc, D. Kundu, L.F. Nazar, Scientific Challenges for the Implementation of Zn-Ion Batteries, Joule 4 (2020) 771–799. https://doi.org/10.1016/j.joule.2020.03.002.

[7] M.E. Spahr, P. Novák, O. Haas, R. Nesper, Electrochemical insertion of lithium, sodium, and magnesium in molybdenum(VI) oxide, J. Power Sources 54 (1995) 346–351. https://doi.org/10.1016/0378-7753(94)02099-O.

[8] X. Sun, P. Bonnick, L.F. Nazar, Layered TiS2 Positive Electrode for Mg Batteries, ACS Energy Lett. 1 (2016) 297–301. https://doi.org/10.1021/acsenergylett.6b00145.

[9] J. Ming, J. Guo, C. Xia, W. Wang, H.N. Alshareef, Zinc-ion batteries: Materials, mechanisms, and applications, Mater. Sci. Eng. R Rep. 135 (2019) 58–84. https://doi.org/10.1016/j.mser.2018.10.002.

[10] J. Song, E. Sahadeo, M. Noked, S.B. Lee, Mapping the Challenges of Magnesium Battery, J. Phys. Chem. Lett. 7 (2016) 1736–1749. https://doi.org/10.1021/acs.jpclett.6b00384.

[11] D.M. Driscoll, S.N. Lavan, M. Zorko, P.C. Redfern, S. Ilic, G. Agarwal, T.T. Fister, R.S. Assary, L. Cheng, D. Strmcnik, M. Balasubramanian, J.G. Connell, Emergent solvation phenomena in non-aqueous electrolytes with multiple anions, Chem (2023) S2451929423001407. https://doi.org/10.1016/j.chempr.2023.03.021.

[12] J.G. Connell, M. Zorko, G. Agarwal, M. Yang, C. Liao, R.S. Assary, D. Strmcnik, N.M. Markovic, Anion association strength as a unifying descriptor for the reversibility of divalent metal deposition in nonaqueous electrolytes, ACS Appl. Mater. Interfaces 12 (2020) 36137–36147.

[13] Ilic, Stefan; Lavan, Sydney; Leon, Noel; Liu, Haoyu; Jain, Akash; Key, Baris; Assary, Rajeev; Liao, Chen; Connell, Justin, Mixed-Anion Contact Ion-Pair Formation Enabling Improved Performance of Halide-Free Mg-Ion Electrolytes, ACS Applied Materials & Interfaces 2024 16 (1), 435-443.

[14] T. Watkins, D.A. Buttry, Determination of Mg^{2+} Speciation in a $TFSI^-$-Based Ionic Liquid With and Without Chelating Ethers Using Raman Spectroscopy, J. Phys. Chem. B 119 (2015) 7003–7014. https://doi.org/10.1021/acs.jpcb.5b00339.

[15] W. Kohn, L.J. Sham, SELF-CONSISTENT EQUATIONS INCLUDING EXCHANGE AND CORRELATION EFFECTS, Phys. Rev. US Superseded Part Phys Rev Phys Rev B Solid State Phys Rev C Phys Rev D Vol: 140 (1965). https://doi.org/10.1103/PhysRev.140.A1133.
[16] P. Hohenberg, W. Kohn, Inhomogeneous Electron Gas, Phys. Rev. 136 (1964) B864–B871. https://doi.org/10.1103/PhysRev.136.B864.
[17] I. Shterenberg, M. Salama, H.D. Yoo, Y. Gofer, J.-B. Park, Y.-K. Sun, D. Aurbach, Evaluation of (CF3SO2)2N− (TFSI) Based Electrolyte Solutions for Mg Batteries, J. Electrochem. Soc. 162 (2015) A7118. https://doi.org/10.1149/2.0161513jes.
[18] A. Khetan, H.R. Arjmandi, V. Pande, H. Pitsch, V. Viswanathan, Understanding Ion Pairing in High-Salt Concentration Electrolytes Using Classical Molecular Dynamics Simulations and Its Implications for Nonaqueous Li–O2 Batteries, J. Phys. Chem. C 122 (2018) 8094–8101. https://doi.org/10.1021/acs.jpcc.8b00944.
[19] M. Herstedt, M. Smirnov, P. Johansson, M. Chami, J. Grondin, L. Servant, J.C. Lassègues, Spectroscopic characterization of the conformational states of the bis(trifluoromethanesulfonyl)imide anion (TFSI−), J. Raman Spectrosc. 36 (2005) 762–770. https://doi.org/10.1002/jrs.1347.
[20] M.J. Monteiro, F.F.C. Bazito, L.J.A. Siqueira, M.C.C. Ribeiro, R.M. Torresi, Transport Coefficients, Raman Spectroscopy, and Computer Simulation of Lithium Salt Solutions in an Ionic Liquid, J. Phys. Chem. B 112 (2008) 2102–2109. https://doi.org/10.1021/jp077026y.
[21] N.T. Hahn, D.M. Driscoll, Z. Yu, G.E. Sterbinsky, L. Cheng, M. Balasubramanian, K.R. Zavadil, Influence of Ether Solvent and Anion Coordination on Electrochemical Behavior in Calcium Battery Electrolytes, ACS Appl. Energy Mater. 3 (2020) 8437–8447. https://doi.org/10.1021/acsaem.0c01070.
[22] N. Sa, N. Nidhi Rajput, H. Wang, B. Key, M. Ferrandon, V. Srinivasan, K. A. Persson, A. K. Burrell, J. T. Vaughey, Concentration dependent electrochemical properties and structural analysis of a simple magnesium electrolyte: magnesium bis(trifluoromethane sulfonyl)imide in diglyme, RSC Adv. 6 (2016) 113663–113670. https://doi.org/10.1039/C6RA22816J.
[23] K. Shimokawa, H. Matsumoto, T. Ichitsubo, Solvation-Structure Modification by Concentrating Mg(TFSA)2–MgCl2–Triglyme Ternary Electrolyte, J. Phys. Chem. Lett. 9 (2018) 4732–4737. https://doi.org/10.1021/acs.jpclett.8b02209.
[24] C. Chang, Y. Yao, R. Li, Z. Cong, L. Li, Z.H. Guo, W. Hu, X. Pu, Stable lithium metal batteries enabled by localized high-concentration electrolytes with sevoflurane as a diluent, J. Mater. Chem. A 10 (2022) 9001–9009. https://doi.org/10.1039/D1TA10618J.
[25] K.S. Han, N.T. Hahn, K.R. Zavadil, N.R. Jaegers, Y. Chen, J.Z. Hu, V. Murugesan, K.T. Mueller, Factors Influencing Preferential Anion Interactions during Solvation of Multivalent Cations in Ethereal Solvents, J. Phys. Chem. C 125 (2021) 6005–6012. https://doi.org/10.1021/acs.jpcc.0c09830.
[26] L.-Q. Chen, Chemical potential and Gibbs free energy, MRS Bull. 44 (2019) 520–523. https://doi.org/10.1557/mrs.2019.162.
[27] Z. Zhao, F. Li, J. Zhao, G. Ding, J. Wang, X. Du, Q. Zhou, G. Hou, G. Cui, Ionic-Association-Assisted Viscoelastic Nylon Electrolytes Enable Synchronously Coupled Interface for Solid Batteries, Adv. Funct. Mater. 30 (2020) 2000347. https://doi.org/10.1002/adfm.202000347.

[28] K.-C. Lau, T.J. Seguin, E.V. Carino, N.T. Hahn, J.G. Connell, B.J. Ingram, K.A. Persson, K.R. Zavadil, C. Liao, Widening Electrochemical Window of Mg Salt by Weakly Coordinating Perfluoroalkoxyaluminate Anion for Mg Battery Electrolyte, J. Electrochem. Soc. 166 (2019) A1510. https://doi.org/10.1149/2.0751908jes.
[29] M. Yang, D.M. Driscoll, M. Balasubramanian, C. Liao, Solvation Structure and Electrochemical Properties of a New Weakly Coordinating Aluminate Salt as a Nonaqueous Electrolyte for Zinc Batteries, J. Electrochem. Soc. 167 (2020) 160529. https://doi.org/10.1149/1945-7111/abcd46.
[30] R. Buchner, G. Hefter, Interactions and dynamics in electrolyte solutions by dielectric spectroscopy, Phys. Chem. Chem. Phys. 11 (2009) 8984–8999. https://doi.org/10.1039/B906555P.
[31] N.T. Hahn, S.A. McClary, A.T. Landers, K.R. Zavadil, Efficacy of Stabilizing Calcium Battery Electrolytes through Salt-Directed Coordination Change, J. Phys. Chem. C 126 (2022) 10335–10345. https://doi.org/10.1021/acs.jpcc.2c02587.
[32] N. Sa, B. Pan, A. Saha-Shah, A.A. Hubaud, J.T. Vaughey, L.A. Baker, C. Liao, A.K. Burrell, Role of Chloride for a Simple, Non-Grignard Mg Electrolyte in Ether-Based Solvents, ACS Appl. Mater. Interfaces 8 (2016) 16002–16008. https://doi.org/10.1021/acsami.6b03193.